The relation between halo shape, velocity dispersion and formation time

C. Ragone-Figueroa,[1,2]★ M. Plionis,[3,4] M. Merchán,[1,2] S. Gottlöber[5] and G. Yepes[6]

[1]*Instituto de Investigaciones en Astronomía Teórica y Experimental, IATE, Observatorio Astronómico, Laprida 854, 5000 Córdoba, Argentina*
[2]*Consejo de Investigaciones Científicas y Técnicas de la República Argentina, Avda. Rivadavia 1917, 1033, Buenos Aires, Argentina*
[3]*Institute of Astronomy & Astrophysics, National Observatory of Athens, Palaia Penteli 152 36, Athens, Greece*
[4]*Instituto Nacional de Astrofísica Optica y Electrónica, AP 51 y 216, 72000 Puebla, México*
[5]*Astrophysical Institute Potsdam, An der Sternwarte 16, 14482 Potsdam, Germany*
[6]*Grupo de Astrofísica, Departamento de Física Teórica, Módulo C-XI, Universidad Autónoma de Madrid, Cantoblanco E-280049, Spain*

ABSTRACT

We use dark matter haloes identified in the MareNostrum Universex and galaxy groups identified in the Sloan Digital Sky Survey Data Release 7 (SDSS DR7) galaxy catalogue to study the relation between halo shape and halo dynamics, parametrizing the mass of the systems. A strong shape–dynamics correlation, independent of mass, is present in the simulation data, which we find to be due to different halo-formation times. Early formation-time haloes are, at the present epoch, more spherical and have higher velocity dispersions than late formation-time haloes. The halo shape–dynamics correlation survives the projection into two dimensions (i.e. between projected shape and 1D velocity dispersion), albeit weaker. A similar shape–dynamics correlation, independent of mass, is also found in the SDSS DR7 groups of galaxies, and in order to investigate its cause we have tested and used, as a proxy of the group formation time, a concentration parameter. We have found, as in the case of the simulated haloes, that less concentrated groups, corresponding to late formation times, have lower velocity dispersions and higher elongations than groups with higher values of concentration, corresponding to early formation times.

Key words: methods: numerical – galaxies: clusters: general – galaxies: haloes – dark matter.

1 INTRODUCTION

According to the hierarchical model of structure formation, groups and clusters of galaxies embedded in dark matter (DM) haloes emerge from Gaussian primordial density fluctuations and grow by accreting smaller structures, formed earlier, along anisotropic directions. Such structures therefore constitute an important step in the hierarchy of cosmic structure formation and are extremely important in deciphering the processes of galaxy and structure formation. It should thus be expected that recently formed structures are highly elongated, reflecting exactly the anisotropic distribution of the large-scale structures from which they have accreted their mass, and dynamically young. Therefore the determination of the dynamical state of groups and clusters of galaxies and its evolution, which could be affected by a multitude of factors such as environment and formation time, is a fundamental step in investigating hierarchical galaxy-formation theories.

Both analytical calculations and N-body simulations have consistently shown that the virialization process will tend to sphericalize the initial anisotropic distribution of matter, and therefore the shape

of haloes is an indication of their evolutionary stage. Furthermore, the halo shape, size and velocity dispersion (amongst others) are important factors in determining halo member orbits and interaction rates, which are instrumental in understanding galaxy formation and evolution processes (e.g. Jing & Suto 2002; Avila-Reese et al. 2005; Bailin & Steinmetz 2005; Kasun & Evrard 2005; Allgood et al. 2006; Bett et al. 2007; Ragone-Figueroa & Plionis 2007; Macció, Dutton & van den Bosch 2008 and references therein). It has been found that DM haloes are triaxial but with a strongly preferred prolateness (e.g. Plionis, Basilakos & Ragone-Figueroa 2006; Gottlöber & Yepes 2007 and references therein) and that there is also a correlation between the orientation of their major axes and the surrounding structures. Such alignment effects have been found to be particularly strong among relatively massive haloes (e.g. Faltenbacher et al. 2002; Hopkins, Bahcall & Bode 2005; Kasun & Evrard 2005; Ragone-Figueroa & Plionis 2007; Faltenbacher et al. 2008 and references therein). There are indications that the above-mentioned correlation might arise, or strengthen, from rearrangements of the orientation of the halo axes in the direction from which the last major merger event occurred (van Haarlem & van de Weygaert 1993). Hence, the shape of DM haloes might well be correlated with the large-scale structure, providing clues to the fashion in which mass is aggregated

★E-mail: cin@mail.oac.uncor.edu

(e.g. Basilakos et al. 2006). The imprints of this accretion can be observed in the substructure features present in a halo, which have been found to correlate with the halo shape (Ragone-Figueroa & Plionis 2007). Haloes with higher levels of substructure, or equivalently dynamically young haloes, are preferentially more elongated. The subsequent evolution should induce a change in the shape of haloes, leading to more spherical configurations and increasing their velocity dispersions as well.

According to this last statement, Faltenbacher & Mathews (2007) have found, in agreement with the Jeans equation, that the velocity dispersion of subhaloes increases with the host halo concentration. Given that halo concentration and formation time are also correlated (Bullock et al. 2001; Wechsler et al. 2002), this result implies that older haloes should have higher subhalo velocity dispersions. Once a halo is virialized, the dynamical mass can be computed from its velocity dispersion and virial radius (e.g. Binney & Tremaine 1987). Nevertheless, if virialization has not yet been achieved, the above-mentioned effect and its possible dependence on the local halo environment should be taken into account. In addition, there is also evidence for the sphericalization of DM haloes with time (e.g. Allgood et al. 2006). This behaviour can be studied well using haloes in numerical simulations, where their three-dimensional (3D) shape and velocity dispersion can be calculated accurately.

These issues motivated us to study the relation between the DM halo velocity dispersion and shape in narrow halo mass ranges, in order to exclude possible halo-mass-dependent effects. We also investigate how this correlation is transformed when computing projected shapes and velocity dispersion along the line of sight, in order to be able to compare our results with observational data, e.g. the SDSS galaxy groups.

The outline of the paper is as follows. In Section 2 we describe the MareNostrum numerical simulation and the SDSS observational data, together with the identification procedure applied to the corresponding systems and their properties. In Section 3 we study the halo shape–dynamics relation in the simulation. In Section 4 we seek a formation-age proxy that can be computed in a realistic group catalogue. We continue in Section 5 by presenting the shape–dynamics correlation results for observed SDSS groups of galaxies. Finally, Section 6 contains our conclusions.

2 HALO AND GROUP DATA

2.1 The MareNostrum simulation

The non-radiative SPH simulation dubbed the MareNostrum Universe (see Gottlöber & Yepes 2007) and covering a volume of $(500 \, h^{-1} \, \mathrm{Mpc})^3$ was performed in 2005 with the parallel TREEPM+SPH Gadget2 code (Springel 2005). The resolution of the simulation is such that the gas and DM components are resolved by 2×1024^3 particles. The initial conditions at redshift $z = 40$ were calculated assuming a spatially flat concordance cosmological model with the following parameters: total matter density $\Omega_\mathrm{m} = 0.3$, baryon density $\Omega_\mathrm{b} = 0.045$, cosmological constant $\Omega_\Lambda = 0.7$, Hubble parameter $h = 0.7$, slope of initial power spectrum $n = 1$ and normalization $\sigma_8 = 0.9$. This resulted in a mass of $8.3 \times 10^9 \, h^{-1} \, \mathcal{M}_\odot$ for the DM particles and $1.5 \times 10^9 \, h^{-1} \, \mathcal{M}_\odot$ for the gas particles. The simulation followed the non-linear evolution of structures in gas and dark matter from $z = 40$ to the present epoch. Dissipative or radiative processes and star formation were not included. The spatial force resolution was set to an equivalent Plummer gravitational softening of $15 \, h^{-1}$ comoving kpc. The

SPH smoothing length was set to the distance to the 40th nearest neighbour of each SPH particle.

After the release of the three-year *WMAP* data, the original simulation was repeated with lower resolution, assuming the predicted low *WMAP*3 normalization ($\sigma_8 = 0.75$), as well as with a higher normalization of $\sigma_8 = 0.8$, which is in better agreement with the five-year *WMAP* data. Yepes et al. (2007) argue that the low-normalization cosmological model inferred from the three-year *WMAP* data results is barely compatible with the present-epoch X-ray cluster abundances. All these simulations have been performed within the MareNostrum Cosmology project at the Barcelona Supercomputer Center.

2.1.1 Halo identification, shape and formation time

In order to find all structures and substructures within the distribution of two billion particles and to determine their properties we have used a hierarchical friends-of-friends (FOF) algorithm (Klypin et al. 1999; Gottlöber et al. 2006b). At all redshifts we have used a basic linking length of 0.17 for the mean interparticle separation to extract the FOF clusters, which corresponds to an overdensity of ∼330 of the mean density. Shorter linking lengths have been used to study substructures. The FOF analysis has been performed independently for DM and gas particles. Using a linking length of 0.17 at redshift $z = 0$, we have identified more than two million objects with more than 20 DM particles that closely follow a Sheth–Tormen mass function (Gottlöber et al. 2006a).

Using the FOF method one extracts rather complex objects, which are characterized by an isodensity surface given by the linking length, from the simulation. To a first approximation these objects can be characterized by triaxial ellipsoids. The shape and orientation of the ellipsoids can be directly calculated as eigenvectors of the inertia tensor of the given object. The shape is then characterized by the ratios between the lengths of the three main axes ($a > b > c$). Gottlöber & Yepes (2007) have studied the shape of galaxy clusters in the MareNostrum Universe and found that both gas and DM components tend to be prolate, although the gas is much more spherically distributed. Here we study the shape of the more massive DM component of the FOF objects, which reflects the shape of the potential in which the galaxies move.

Finally, in our present work we will extensively use the notion of halo-formation time (z_form), which is usually defined as the redshift at which the halo accretes half of its final ($z = 0$) mass. By selecting haloes in the lower and upper quartiles of the formation-time distribution, we define what we will call the late formation-time (LFT) and early formation-time (EFT) halo populations, respectively. We also divide the haloes into four mass ranges, namely 1.0–1.3, 2.0–2.5, 3.2–4.0 and 6.3–7.9 $\times 10^{13} \, h^{-1} \, \mathcal{M}_\odot$, since we wish to cancel the dependence of any halo-based parameter on its mass.

Fig. 1 shows the distribution of formation times for the four subsamples of haloes as defined previously. The vertical dashed lines denote the location of the first and fourth quartiles of the distribution.

2.2 SDSS DR7 galaxy groups

In recent years considerable effort has been invested in identifying, using a multitude of methods, groups and clusters of galaxies in redshift surveys (e.g. Huchra & Geller 1982; Nolthenius & White 1987; Tully 1987; Merchán & Zandivarez 2002, 2005; Ramella et al. 2002; Gal et al. 2003; Eke et al. 2004; Gerke et al. 2005; Lee
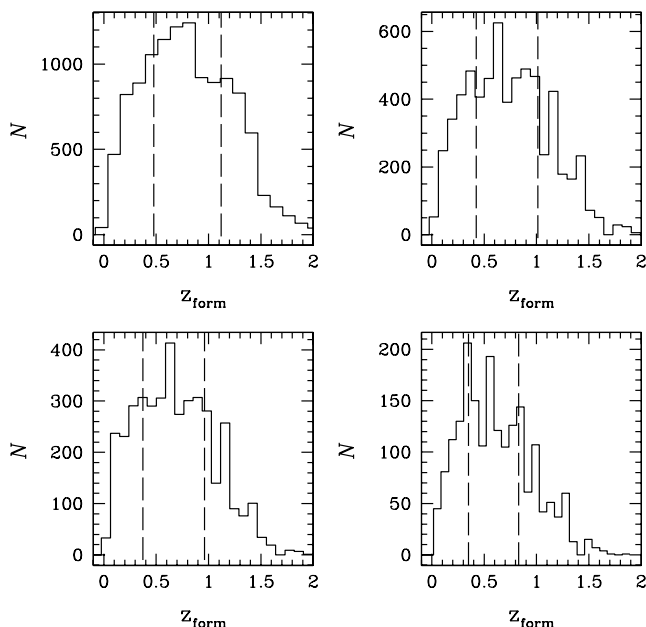
Figure 1. Different panels correspond to the formation-time distribution of haloes in different mass ranges, namely 1.0–1.3, 2.0–2.5, 3.2–4.0 and 6.3–7.9 $\times 10^{13}\, h^{-1}\, \mathcal{M}_\odot$, from left to right and top to bottom. Vertical dashed lines denote the first and fourth quartiles of the distribution.
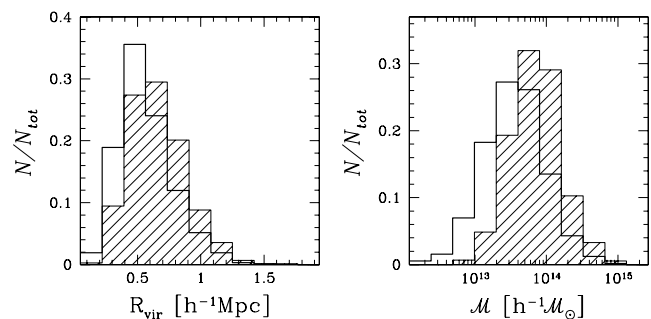

Figure 2. Fractional distribution of virial radii (left panel) and masses (right panel) of groups in a volume-limited sample (with 10 or more members) extracted from SDSS DR7, corresponding to $0.06 < z < z_{\rm lim} = 0.10$ (dashed histogram), compared with that for the total sample of groups (with three or more members) up to $z = 0.10$ (empty histogram).

et al. 2004; Lopes et al. 2004; Berlind et al. 2006; Tago et al. 2006, 2008; Crook et al. 2007; Yang et al. 2007; Finoguenov et al. 2009; Sharma & Johnston 2009).

In this work we identify groups of galaxies in the SDSS DR7 spectroscopic galaxy sample, which comprises more than 900 000 galaxies within an area of approximately 9000 deg^2 and with a limiting r-band magnitude of $m_{\rm lim} = 17.77$. The group-finding algorithm is based on the procedure detailed in Merchán & Zandivarez (2005) and consists of using the FOF algorithm, similarly to the process developed by Huchra & Geller (1982). The algorithm links galaxies (i and j) that satisfy $D_{ij} \leq D_0 R(z)$ and $V_{ij} \leq V_0 R(z)$, where D_{ij} is their projected distance and V_{ij} is their line-of-sight velocity difference. The scaling factor $R(z)$ is introduced in order to take into account the decrement of the galaxy number density due to the apparent magnitude-limit cut-off. We have adopted a transverse linking length D_0 corresponding to an overdensity of $\delta\rho/\rho = 80$ and a line-of-sight linking length of $V_0 = 200\,{\rm km\,s}^{-1}$.

In order to avoid significant discreteness effects in the group shape and dynamics determination, we limit our catalogue to those groups with more than 10 members ($n_{\rm m} \geq 10$). To further avoid artificial redshift-dependent effects (e.g. Plionis, Basilakos & Tovmassian 2004; Frederic 1995; Plionis et al. 2006) and to build a roughly volume-limited sample, we select those groups with $0.06 < z < 0.1$ and $M_{10} < M_{\rm lim}$, where M_{10} is the absolute magnitude of the tenth brightest galaxy and $M_{\rm lim}$ ($= -19.53$) is the absolute magnitude of a galaxy with apparent magnitude $m = m_{\rm lim}$ at $z = 0.1$. The resulting sample, within the previously mentioned z range, comprises 760 groups with at least 10 member galaxies.

For these groups, we compute their virial radius, line-of-sight velocity dispersion (σ_z) and virial mass ($\mathcal{M}$), following Merchán & Zandivarez (2005). In Fig. 2 we present the distribution of virial masses and radii of the resulting groups, comparing our results with those of the whole ($n_{\rm m} \geq 3$ and $z < 0.1$) parent-group sample. It is evident that we are preferentially selecting the richest systems,

which is the price we have to pay for producing a volume-limited subsample.

2.2.1 Group projected shape

The group elongation is determined by diagonalizing the 'inertia' tensor, which we construct by weighting each galaxy n by its luminosity L_n. This is done in order to assign more weight to the galaxies that dominate in shaping the group gravitational potential:

$$I_{ij} = \sum_{n=1}^{10} L_n\, x_{i,n}\, x_{j,n},\qquad(1)$$

where $x_{i,n}$ is the ith component of the position vector of the nth galaxy relative to the group centre of mass. Diagonalizing the I_{ij} tensor, we obtain two eigenvalues related to the square roots of the minor and major axes, b and a respectively, which define the halo axial ratio $q = b/a$.

Furthermore, as is well documented, there exists a dependence of the group halo apparent elongation on the member-number resolution of the system (e.g. Paz et al. 2006; Plionis et al. 2006). According to this effect, a given system will appear artificially more elongated (smaller $q = b/a$ ratio) when sampled by a lower number of members. This effect, however, is large for groups with less than 10 members (see fig. 3 in Plionis et al. 2006) and therefore it should not affect our group sample, which by construction has $n_{\rm m} \geq 10$, significantly. In any case, and to overcome any residual effect that could be introduced due to the variable resolution of the different groups, we sample each group having $n_{\rm m} > 10$ by selecting randomly only 10 galaxies, the number resolution of the lowest $n_{\rm m}$ galaxy groups in our sample. Finally, the adopted value of the projected shape, $q_{\rm ran}$, is the result of computing the mean of 10 realizations of the random galaxy selection procedure. *By this procedure we degrade the accuracy of the shape parameter of groups with $n_{\rm m} > 10$, but we gain resolution consistency over our whole group sample.* To get an idea of the uncertainty introduced by our procedure, we present in the left panel of Fig. 3 the q versus $q_{\rm ran}$ correlation. As expected, the $q_{\rm ran}$ values are systematically lower than their counterparts q computed using all member galaxies, while the deviation increases for intrinsically more spherical systems. Since in this plot we show all groups with $n_{\rm m} \geq 20$, in the right panel of Fig. 3 we plot the median value of $q - q_{\rm ran}$ as a function of the minimum number of group member galaxies. It can be seen than there is, as expected, a tendency of $q - q_{\rm ran}$ to increase slowly with $n_{\rm m}$ but, within the errors, we can quote an overall median value of $\overline{q - q_{\rm ran}} \simeq 0.063 \pm 0.035$, independent of $n_{\rm m}$.
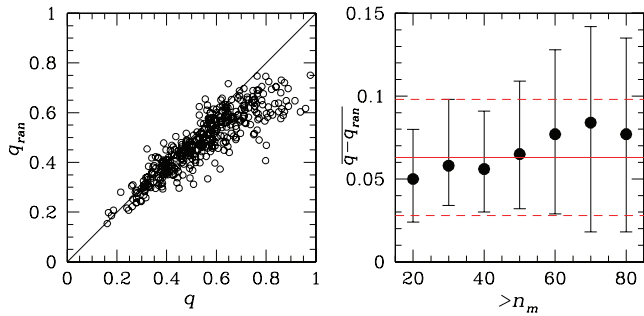
Figure 3. Left: the $q - q_{ran}$ scatter plot for groups within the volume-limited sample and with at least 20 member galaxies. Right: the median value of $q - q_{ran}$ as a function of the minimum number of group galaxy members. Error bars correspond to the 33 per cent and 67 per cent quantiles. The solid line corresponds to the value $q - q_{ran} = 0.063$ and the dashed lines to the ± 0.035 range.

3 THE HALO SHAPE–DYNAMICS RELATION

In this section we investigate the relation between morphology and dynamical status of DM haloes.

As is well known, halo properties can have a strong dependence on halo mass. In particular, the velocity dispersion of virialized or nearly virialized haloes is related to the halo mass through the virial theorem: $M \propto \sigma^2$. Therefore, in order to search for an intrinsic dependence of the velocity dispersion on shape it is imperative to suppress the possible dependence on mass due to the virialization expectation. To this end we have studied the shape–σ_v correlation in the four mass ranges defined in Section 2.1.2, both in 3D space and in projected 2D space (using 1D velocities and projected halo shapes).

3.1 3D halo c/a–σ_v correlation

Fig. 4 shows the isodensity contours of the shape–σ_v scatter plot at redshift $z = 0$ for some of the selected mass bins (left boxes of each panel). As can be seen, there exists a clear correlation between halo sphericity and halo velocity dispersion, according to which more spherical haloes have higher velocity dispersions. Even though we have been cautious in selecting small mass ranges, the observed behaviour could, in principle, be attributed to the halo-mass variation within each mass bin. For this to be true the more massive systems within each bin – which should also have the higher velocity dispersions – should have the highest values of the c/a ratio. However, it is well established that more massive systems tend to be less spherical (e.g. Allgood et al. 2006). Therefore, the observed
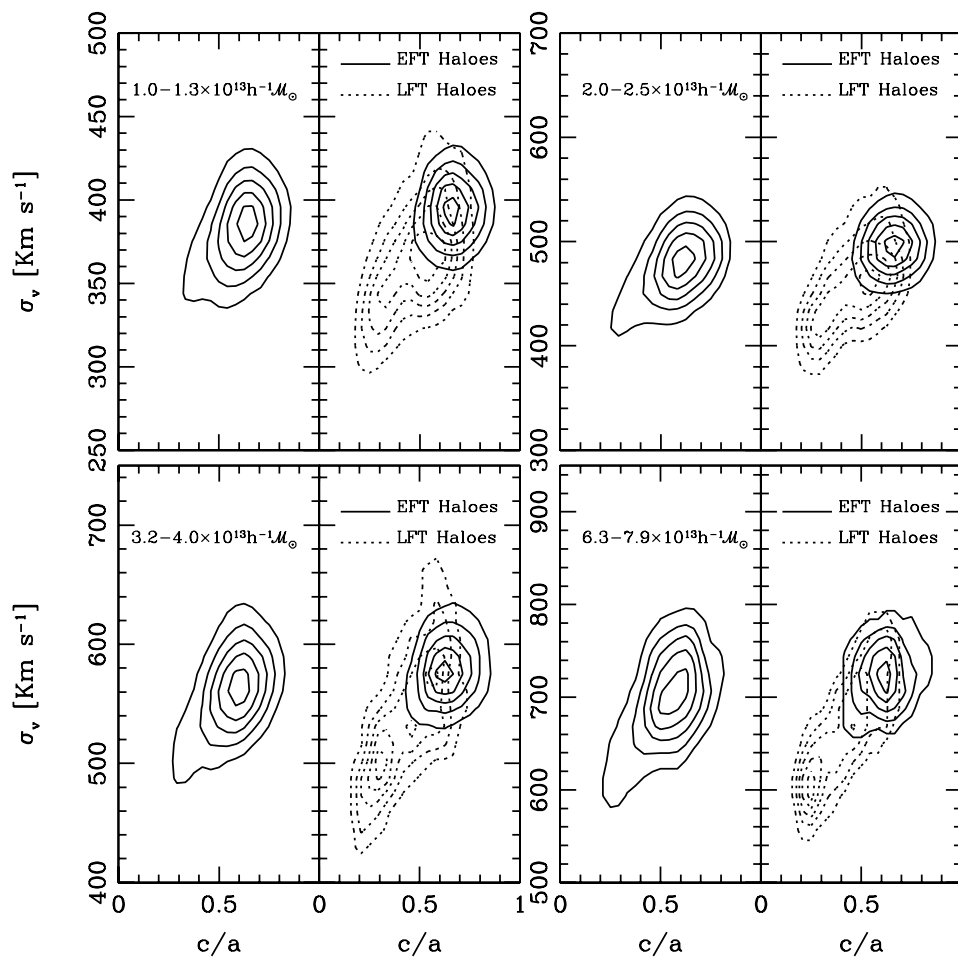

Figure 4. Each panel corresponds to haloes in the four different ranges of mass, increasing in mass from top left to bottom right. The left part of each panel shows the isodensity contours of c/a versus σ_v for all haloes in the corresponding range of mass. The right part of each panel shows the corresponding isodensity contours, but only of the 25 per cent and 75 per cent quantiles of the formation-time distribution, which correspond to the EFT (solid line) and LFT (dotted line) families of haloes.

correlation cannot be attributed to a possible residual dependence on halo mass. A rather interesting possibility is related to the fact that haloes of any given mass and at any given cosmic epoch could have different formation times as well as different evolutionary histories.

Under this hypothesis, and in order to investigate further the dependence of the shape–σ_v correlation on the halo-formation time (z_{form}), we plot the EFT and LFT c/a–σ_v correlations separately in the right-hand half of each panel of Fig. 4. It is evident that the two populations occupy clearly delineated regions in the c/a–σ_v plane, with the EFT haloes (solid line) typically having higher velocity dispersions and higher sphericities than the LFT haloes (dotted line). One can also observe that the LFT contours cover a wider range of σ_v values than the corresponding EFT ones, but do not reach the highest EFT sphericities. Finally, it is also interesting to note that there is a shift in the peak of the LFT contours towards lower c/a and σ_v values between the lower mass (upper panels) and higher mass (lower panels) LFT haloes. This could be attributed to a fraction of the most massive LFT systems being relatively more dynamically young and in the phase of primary mass aggregation. We will return to this issue later on.

As is obvious from Fig. 4, the same overall trend between the LFT and EFT haloes is present in all mass bins. It would therefore be ideal, in order to enhance the statistical validity of our results, to combine the information contained in the different mass ranges in a unique analysis independent of halo mass. This would also facilitate a corresponding study of the observational data, since the available number of SDSS groups is significantly smaller than that of the simulated haloes and thus we cannot afford to divide them into many mass subsamples.

Since the parameters under study (σ_v, c/a and z_{form}) depend on halo mass, we have devised a normalization procedure that imposes the mass independence of the results and combines the halo velocity dispersion and shape of the whole sample in a unique relation. In more detail, we derive normalization functions of the different parameters by computing analytic fits of the relation between the corresponding parameter (P) and the halo mass ($\mathcal{M}$). Then for a given halo mass we normalize each of the three parameters under study to the value expected from the analytic fit ($\overline{P(\mathcal{M})}$).

Since it is no longer necessary to split haloes into narrow mass bins, we can use the entire main sample of haloes to plot in Fig. 5 the normalized shape–dynamics correlation independent of mass. It is evident that the EFT and LFT behaviour seen in Fig. 4 is reproduced for the whole halo sample and we have further verified that these results are indeed independent of halo mass. In the inset of Fig. 5 we show that the corresponding distributions of masses of the EFT (solid line) and LFT (dashed line) populations are statistically equivalent and therefore there is no residual mass-dependent effect affecting the correlation shown in the main panel.

Our main results, as extracted from Figs 4 and 5, can be summarized as follows. (i) The LFT haloes show a significantly stronger c/a–σ_v correlation than the EFT haloes, while they also span a wider range of values. (ii) The LFT σ_v values are, in some cases, even higher than those of the EFT ('virialized') halo population. (iii) A bimodal pattern is present in the σ_v–c/a plane (Fig. 5) with two local maxima, one of which is situated at low velocity-dispersion and low c/a values, which as we have discussed earlier and deduced from Fig. 4 result from more massive haloes. Below we attempt to interpret each of the above results individually.
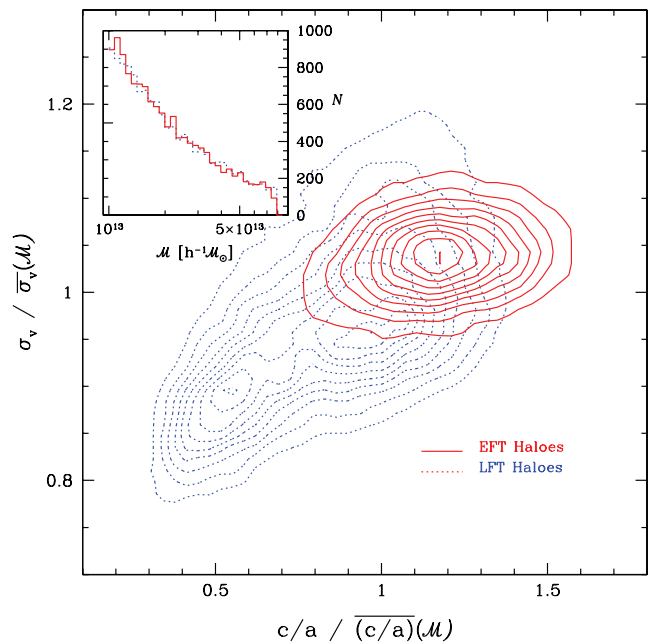

Figure 5. Normalized c/a–σ_v relation for EFT (solid line) and LFT (dashed line) populations. All masses are considered. The formation time used to divide EFT and LFT is also normalized to the expected value for a given mass (see text). *Inset panel*: distribution of masses of EFT (solid line) and LFT (dashed line) populations, demonstrating that no mass effect is present in the result obtained in the main panel.

3.1.1 Case (i): different σ_v–c/a correlation strength of the EFT and LFT haloes

The apparent lack of a strong correlation of the EFT halo population should be attributed to the fact that EFT haloes have had plenty of time to virialize and that the virialization process erases the intrinsic shape–σ_v correlation. To quantify the strength of the shape–σ_v correlation we estimate the Spearman correlation coefficient as a function of halo mass (Table 1). Clearly, the observed strong and significant correlation of the whole halo population should be attributed to the LFT haloes, since (as we already discussed) the EFT haloes show very weak shape–σ_v correlations.

So far, the results obtained suggest that the intrinsic halo shape–σ_v correlation, within each small mass range, is the consequence of the coexistence of haloes of different formation times and going

Table 1. The Spearman coefficient (SC) for the velocity dispersion–shape correlation for haloes in four mass bins. In all cases (3D and 2D) the correlations of the EFT haloes are significantly lower than those of the LFT haloes.

Sample	Mass [$\times 10^{13} \mathcal{M}_\odot\, h^{-1}$]			
	1.0–1.3	2.0–2.5	3.2–4.0	6.3–7.9
3D All	0.37	0.42	0.44	0.48
3D LFT	0.45	0.55	0.60	0.72
3D EFT	0.11	0.16	0.21	0.22
2D All	0.27	0.31	0.33	0.34
2D LFT	0.31	0.38	0.42	0.47
2D EFT	0.11	0.12	0.15	0.18

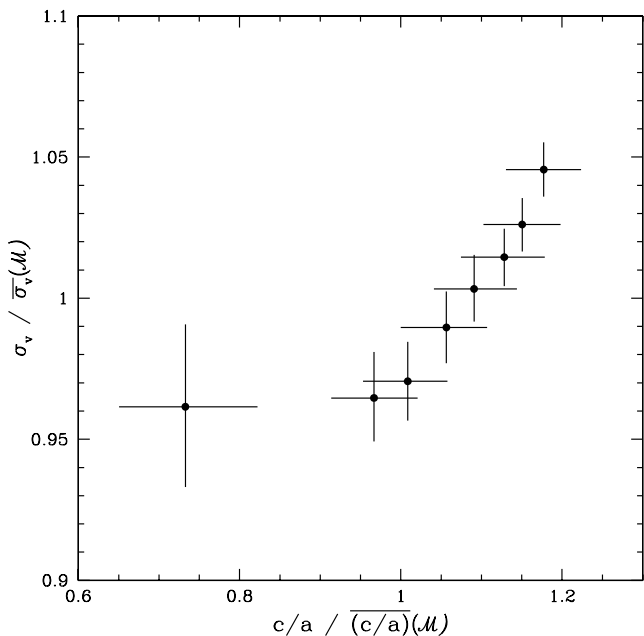**Figure 6.** Normalized c/a–σ_v trend corresponding to the entire sample of haloes. Each point corresponds to the median $c/a/[\overline{(c/a)}(\mathcal{M})]$ and $\sigma_v/[\overline{\sigma_v}(\mathcal{M})]$ values computed for haloes with z_{form} within different octiles of formation time. Error bars mark the 10 per cent percentile of the corresponding distribution.

through different evolutionary phases.[1] DM haloes, in the initial stages of formation and before virialization is complete, typically have a smaller velocity dispersion and a more elongated shape. Once virial equilibrium is reached these quantities stabilize and, since this equilibrium configuration is more likely to be achieved by EFT haloes, the EFT family shows only a weak shape–σ_v correlation.

We attempt to investigate the evolution paradigm as the cause of the σ_v–c/a correlation in more detail, by dividing the halo formation-time distribution into eight quantiles. We then compute the median values of $\sigma_v/[\overline{\sigma}(\mathcal{M})]$ and $c/a/[\overline{(c/a)}(\mathcal{M})]$ within each z_{form} quantile and plot them in Fig. 6. In concordance with Fig. 5, we consistently find a clear trend indicating that the earlier the halo is formed the higher its σ_v and c/a ratio, as expected from the fact that older haloes have more time to evolve and virialize. Evidently a halo evolutionary sequence appears, with dynamically young haloes situated at the lower left of the c/a–σ_v plane; as they evolve they move towards higher σ_v and c/a values, where the virialized haloes are located.

Note, however, that in Fig. 6 the dynamically youngest haloes (first octile of formation time) show a behaviour that deviates from the overall trend, being characterized by a lower normalized c/a value. This outlier has a relatively larger uncertainty with respect to the other octiles, and a possible cause of this behaviour is presented in the discussion of case (iii).

3.1.2 Case (ii): LFT haloes with σ_v values even larger than those of EFT haloes

In an attempt to explain the cause of the rather unexpected behaviour of some LFT haloes, i.e. those having relatively high sphericity and

at the same time a velocity dispersion as large as or even larger than expected from 'virialized' EFT haloes, we suggest two mechanisms.

(1) Since LFT haloes are prone to have had a recent merger and since it is expected that dynamical interactions and merging processes increase the velocity dispersion of the involved systems, some merging or highly interacting haloes could be undergoing a transient geometrical configuration of high sphericity (resulting when the infalling substructures are near the perigee), while temporarily achieving a velocity dispersion that could be even larger than their virial value (Faltenbacher, Gotlöber & Mathews 2006). We have verified that this is indeed the case for some of the LFT haloes.

(2) Some of the high-velocity-dispersion and quasi-spherical LFT haloes could arise from truly virialized LFT haloes by a somewhat rapid virialization process depending on their particular formation history and/or environment.

3.1.3 Case (iii): the two maxima in the LFT σ_v–c/a correlation plane

As we have discussed earlier, the lower σ_v–c/a maximum seen in Fig. 5 is caused by the most massive haloes (i.e. those with $\mathcal{M} \gtrsim 3.2 \times 10^{13} \, h^{-1} \, \mathcal{M}_\odot$) and could be attributed to a fraction of the most massive LFT systems being relatively dynamically younger and in the phase of merging, where the FOF algorithm could join a merging pair into a single FOF halo.

In order to verify our suspicion, we have selected haloes with masses in range 3.2–$7.9 \, h^{-1} \, \mathcal{M}_\odot$ (including the two most massive ranges presented in Fig. 4, where the bimodal pattern was evident for the LFT haloes) and investigated in what manner the described trend would be affected if double- (or multiple-)core haloes (or otherwise dumbbell-shaped haloes) were excluded. Double-core haloes were identified as those haloes that are split into two or more subhaloes of at least 1000 particles, within a relative distance of $2r_{sph}$ (r_{sph} is the diameter of a sphere that has the same volume as the halo considered), when a re-identification with a shorter linking length (0.135 of the mean interparticle separation) is performed. Therefore, they are major pre-merger systems joined by the FOF into a single system, for which other halo-finders would probably have singled out each component as an individual halo. In the left panel of Fig. 7 we show the c/a–σ_v correlation when all haloes in the mass range mentioned are considered, whereas in the right panel double-core haloes are excluded. It is evident that the secondary maximum at low σ_v and c/a is caused by double-core haloes, which are those that are in an active major merger process and thus an
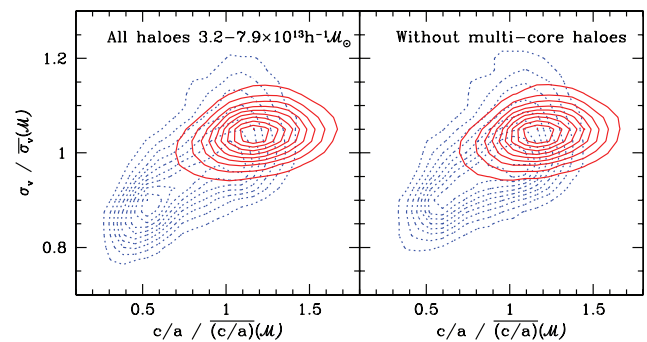

Figure 7. Same as Fig. 5, but only considering haloes with masses between 3.2 and $7.9 \times 10^{13} \, h^{-1} \, \mathcal{M}_\odot$. In the left panel the entire sample is used whereas in the right panel all double-core haloes have been excluded.

[1] Note that a similar conclusion was reached in a recent observational study of $z \lesssim 0.04$ groups of galaxies (Tovmassian & Plionis 2009).
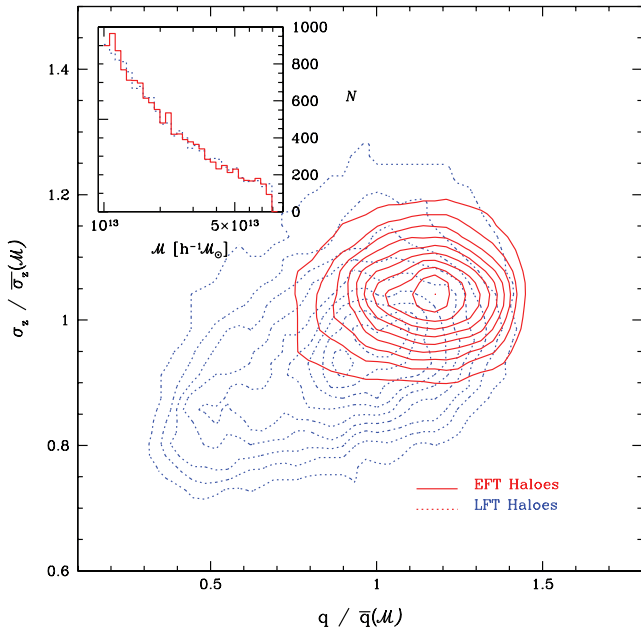
Figure 8. As in Fig. 5 but using projected halo shapes and 1D velocity dispersions.

Figure 9. The $\Delta_{\rm subh}$ parameter as a function of formation time computed for dark matter haloes in four ranges of halo mass.

integral part of the 'dynamically young' family of haloes. Note that although the c/a–σ_v LFT correlation is weakened when the double-(multiple-)core haloes are excluded, it is still clearly present.

Returning to the issue of the 'outlier' seen in Fig. 6, we have verified that the cause of the significantly smaller normalized $\langle c/a \rangle$ value of the first formation-time octile is the significantly larger number of double- (multiple-)core haloes found in this octile with respect to the other octiles. For example, for the case of the most massive haloes (i.e. those investigated in Fig. 7) we find that ∼22 per cent of the haloes in the first octile are double- (multiple-)core haloes, while this number drops to 4.8 and 2.6 per cent in the second and third octiles respectively, and to even smaller values thereafter.

3.2 2D Halo q–σ_z correlation

Here we present the analysis corresponding to the previous subsection, but using the projected halo axial ratio ($q = b/a$ obtained from the projected particle distribution) and the 1D velocity dispersion. This is done in order to see how the previous (3D) results are translated into theoretical expectations that can be compared with the results based on observational group samples.

Fig. 8 is the 2D analogue of Fig. 5 and we can clearly see that qualitatively the correlation revealed in Fig. 5, albeit weaker, is repeated in Fig. 8. Details and significances may differ (see Table 1 for different mass ranges), however, the main result is that we expect to see (in realistic group samples) hints of an independence of mass correlation of the projected halo axial ratio with its line-of-sight velocity dispersion.

4 A FORMATION-TIME PROXY

The aim of this section is to provide a formation-age proxy, tested with simulated haloes but one that can also be computed for realistic groups of galaxy samples, where the adopted definition of $z_{\rm form}$ is not usable. This is done in order to test the morphology–dynamics–
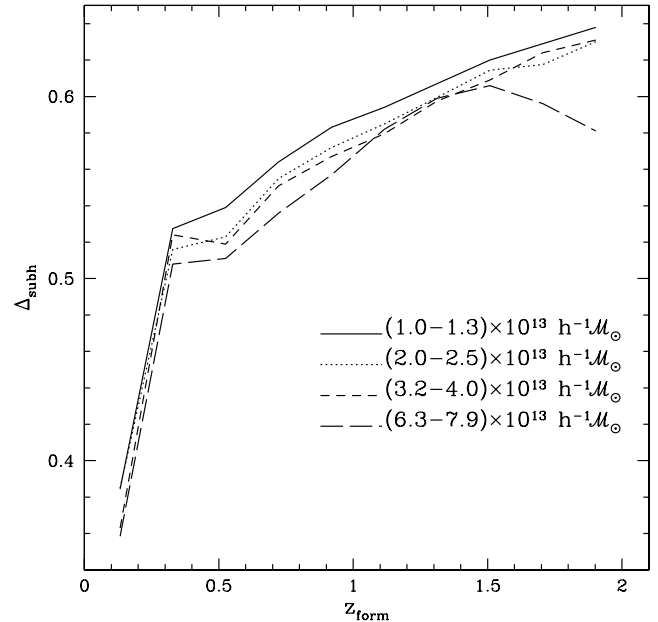
formation time correlation (which was found to be present in simulated haloes) in groups extracted from the SDSS DR7.

We propose as a halo formation-age proxy ($\Delta_{\rm subh}$) the fraction of mass that is associated with the most massive substructure (sub-halo), when a further re-identification is performed with a linking length that equals half the original one (0.17/2 of the mean interparticle separation). This proposed parameter can be interpreted as a concentration indicator, since it accounts for the distribution of mass at two different overdensities (given by the linking lengths used).

The number of halo particles at each overdensity level is defined as $n_{\rm high}$ and $n_{\rm low}$ for the higher and lower overdensities, respectively. Then the concentration parameter is given by

$$\Delta_{\rm subh} = \frac{n_{\rm high}}{n_{\rm low}} \ . \tag{2}$$

The parameter $\Delta_{\rm subh}$ takes values within the range $\Delta_{\rm subh} \in [0, 1]$, with a value near 1 indicating a high concentration and a value near 0 indicating the opposite. We show in Fig. 9 the relation between $\Delta_{\rm subh}$ and halo-formation redshift for the different ranges of mass labelled in the plot. It is evident that the oldest haloes have the highest levels of concentration, whereas the youngest ones extend to lower values of $\Delta_{\rm subh}$.

Since the above analysis clearly demonstrates that the proposed parameter can be used as an age indicator, we continue with the computation of the concentration parameter corresponding to galaxy groups in the observational data, $\Delta_{\rm sub}$. To this end we perform a second FOF identification, but this time using an overdensity of $\delta\rho/\rho = 300$. This procedure allows us to extract a denser subgroup of a given system with respect to the original $\delta\rho/\rho = 80$ sample. Then $\Delta_{\rm sub}$ is given by the ratio between the number of members of the denser subgroup to the number of members of its parent ($\delta\rho/\rho = 80$) group. Utilizing this formation-age proxy, we examine the SDSS-DR7 group shape–dynamics–formation time relation in the next section.

5 THE SHAPE–VELOCITY DISPERSION RELATION OF SDSS DR7 GROUPS

Many studies have attempted to determine the morphology and dynamical status of groups of galaxies (e.g. Hickson et al. 1982; Malykh & Orlov 1986; Orlov, Petrova & Tarantaev 2001; Kelm & Focardi 2004; Plionis et al. 2004, 2006; Coziol & Plauchu-Frayn 2007; Wang et al. 2008; Hou et al. 2009) and have found that their morphology corresponds to that of mostly prolate-like triaxial ellipsoids (see however Robotham, Phillips & de Propris 2007), while there also appears to be a correlation between velocity dispersion and projected group shape (e.g. Tovmassian & Plionis 2009), similar to that found in the previous section.

Here we analyse our 'volume-limited' group catalogue based on the SDSS DR7 galaxy survey, which was described in Section 2.

As we have concluded in Section 3.2, the shape–σ correlation for DM haloes extracted from the simulation survives in projection but it is significantly weakened when the projected shape (q) and 1D velocity dispersion are used. Further scatter should be expected in a more realistic situation in which the projected shapes of SDSS groups are computed using only 10 members (q_{ran}). Indeed, as was shown in Section 2.2, the typical error expected when only 10 members are considered in the estimation of the projected shape is non-negligible. Such issues may act to hide the morphology–dynamics correlation of observed groups of galaxies, and thus even a weak correlation should be considered as the hint of a true underlying effect. We show in Fig. 10 the least-squares best-fitting line of the q_{ran} versus $\sigma_z/\bar{\sigma}_z(\mathcal{M})$ scatter plot (of the entire sample of galaxy groups), where the observed trend is in full agreement with Fig. 8.

We now attempt to investigate whether the observed q_{ran} versus σ_z correlation in Fig. 10 is due to the coexistence of groups with different formation times, as was indeed shown to be the case in the DM halo analysis. As shown in Section 3.2 (see also Fig. 8), using
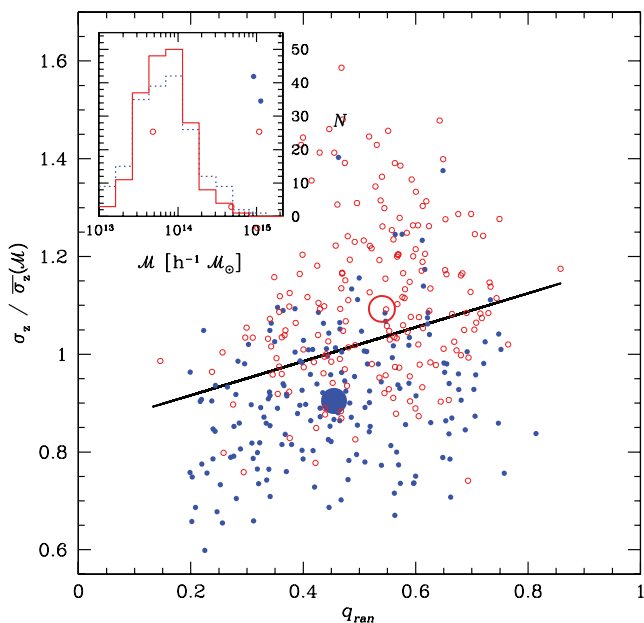

Figure 10. q_{ran} versus normalized σ_z relation for groups in SDSS DR7. Filled (low concentration) and empty (high concentration) dots stand for groups in the first and last quartiles of the normalized Δ_{sub} distribution, respectively. The large circles correspond to the median values. The solid line shows the least-squares fit using all groups, irrespective of their Δ_{sub} value. The inside box shows the mass distributions for groups in the quartiles of low and high concentration (dotted and solid lines respectively).

projected shapes and 1D velocity dispersions does not completely mask the systematic behaviour observed for haloes with different formation times. However, taking into account the unfeasibility of determining the formation time of the observed galaxy groups, we use as a proxy of the group dynamical age its concentration parameter Δ_{sub}. This parameter has indeed been shown (for the case of DM haloes) to correlate with halo-formation time (see Section 4).

In Fig. 10 we separately plot groups from the first and last quartiles of the Δ_{sub} parameter distribution (as was done for formation time in Section 3.1). Filled and empty circles represent galaxy groups with low and high concentrations (corresponding to groups in the first and last quartiles of the Δ_{sub} distribution), respectively. The tendency for high-concentration groups (open circles) to have systematically higher velocity dispersions and q values is quite evident. We also plot their corresponding median values as large filled and empty circles, from which it can be seen that indeed there is a separation of the two families (based on Δ_{sub}) in both q_{ran} and σ_z axes. We have again verified that the observed behaviour is not due to a mass-dependent effect, since the distributions of mass of the two group families are statistically equivalent (see insert of Fig. 10).

It is important to keep in mind that the uncertainty in the determination of the projected group shape, induced by our random sampling procedure aimed at reducing variable resolution effects, could introduce a large scatter in the morphology–dynamics correlation. This could then act to hide the differences between the two families of groups represented by the different symbols in Fig. 10. We have tested this assertion by using, within small ranges of group mass and for a given number of galaxy members, all available galaxy members to estimate the group q values more accurately, at the expense of working with a low number of groups. We now find significantly larger differences between the mean q values of the low- and high-concentration families. Therefore, had we higher resolution measurements of group shapes we would have recovered a significantly larger separation between the low- and high-concentration group families in the $q–\sigma_z$ plane, strengthening the interpretation of group formation-time differences being the cause of the observed $q–\sigma_z$ correlation, as is the case in the DM haloes analysed.

6 SUMMARY AND CONCLUSIONS

We have identified dark matter haloes in the MareNostrum Universe and groups of galaxies in SDSS DR7 with the purpose of searching for possible dependences of halo/galaxy-group shape on dynamics, independent of mass.

We have computed the halo-formation time as the redshift at which the halo accretes half of its final mass. Since this definition of formation time is not applicable to observed groups identified in realistic galaxy catalogues, we have identified a concentration parameter that can be used as a proxy for the formation time of haloes and at the same time can be easily computed for the observed SDSS galaxy systems.

With this regard, we have found a significant correlation between halo shape and dynamics (velocity dispersion) that is independent of the halo mass. We have identified the cause of this correlation to be halo-formation-time differences. Early formation-time haloes show a very weak correlation, as they are more spherical, have a higher velocity dispersion and show substantial concentration. In contrast, late formation-time haloes show a strong shape–dynamics correlation (having a wide range of shape and velocity-dispersion values), with typically lower velocity dispersions, lower sphericities and significantly lower concentrations. We have also studied the influence of multicore haloes (i.e. major merger systems joined by

the FOF into a single system for which other halo-finders would have probably singled out each component) on the strength of the LFT shape–dynamics correlation and verified that although such haloes enhance the correlation, this however persists even when this subsample of haloes is excluded.

Finally, we find that a fraction of the LFT haloes show somewhat unexpected behaviour, having high sphericities and velocity dispersions (comparable to or even higher than those of more virialized systems), a fact that could be attributed to either some late formation-time haloes having transitory spherical shapes and large velocity dispersion during the minimum pericentric passage of a merging process, or/and to a relatively faster virialization process occurring in some of these haloes.

The halo morphology–velocity-dispersion correlation survives the 2D projection, albeit more weakly, indicating that analogous behaviour should be expected in observational group samples. Applying a similar analysis to a 'volume-limited' subsample of SDSS DR7 groups of galaxies, identified using a FOF algorithm, we have also found a group shape and dynamics correlation that is independent of group mass (see also Tovmassian & Plionis 2009). Using a concentration parameter as a proxy for the formation time, we indeed find a significant shape–dynamics correlation, independent of mass, in a similar fashion to the dark matter halo case. Less concentrated (late-forming) groups are typically less spherical and have lower velocity dispersions than their equal-mass more concentrated (early-forming) counterparts.

ACKNOWLEDGMENTS

REFERENCES

Allgood B., Flores R. A., Primack J. R., Kravtsov A. V., Wechsler R. H., Faltenbacher A., Bullock J. S., 2006, MNRAS, 367, 1781
Avila-Reese V., Colín P., Gottlöber S., Firmani C., Maulbetsch C., 2005, ApJ, 634, 51
Bailin J., Steinmetz M., 2005, ApJ, 627, 647
Basilakos S., Plionis M., Yepes G., Gottlöber S., Turchaninov V., 2006, MNRAS, 365, 539
Berlind A. A. et al., 2006, ApJS, 167, 1
Bett P., Eke V., Frenk C. S., Jenkins A., Helly J., Navarro J., 2007, MNRAS, 376, 215
Binney J., Tremaine S., 1987, Galactic Dynamics. Princeton Univ. Press, Princeton
Bullock J. S., Kolatt T. S., Sigad Y., Somerville R. S., Kravtsov A. V., Klypin A. A., Primack J. R., Dekel A., 2001, MNRAS, 321, 559
Coziol R., Plauchu-Frayn I., 2007, AJ, 133, 2630
Crook A. C., Huchra J. P., Martimbeau N., Masters K., Jarrett T., Macri L. M., 2007, ApJ, 655, 790

Eke V. R. et al., 2004, MNRAS, 348, 866
Faltenbacher A., Mathews W. G., 2007, MNRAS, 375, 313
Faltenbacher A., Gottlöber S., Kerscher M., Müller V., 2002, A&A, 395, 1
Faltenbacher A., Gotlöber S., Mathews G., 2006, preprint (astro-ph/0609615)
Faltenbacher A., Jing Y. P., Li C., Mao S., Mo H. J., Pasquali A., van den Bosch F. C., 2008, ApJ, 675, 146
Finoguenov A. et al., 2009, ApJ, 704, 564
Frederic J. J., 1995, ApJS, 97, 259
Gal R. R., de Carvalho R. R., Lopes P. A. A., Djorgovski S. G., Brunner R. J., Mahabal A., Odewahn S. C., 2003, AJ, 125, 2064
Gerke F. B. et al., 2005, ApJ, 625, 6
Gottlöber S., Yepes G., 2007, ApJ, 664, 117
Gottlöber S., Yepes G., Wagner C., Sevilla R., 2006a, in Tresse L., Maurogordato S., Tran Than Van J., eds, Proceedings of the XLIst Rencontres de Moriond, XXVIth Astrophysics Moriond Meeting: From Dark Halos to Light. The Gioi Publishers, Hanoi, pp. 309–314
Gottlöber S., Yepes G., Khalatyan A., Sevilla R., Turchaninov V., 2006b, in Munoz C., Yepes G., eds, AIP Conf. Proc. Vol. 878, Proceedings of the DSU2006 conference. Am. Inst. Phys., New York, pp. 3–9 (astro-ph/0610622)
Hickson P., 1982, ApJ, 255, 382
Hopkins P. F., Bahcall N. A., Bode P., 2005, ApJ, 618, 1
Hou A., Parker L. C., Harris W. E., Wilman D. J., 2009, ApJ, 702, 1199
Huchra J. P., Geller M. J., 1982, ApJ, 257, 423
Jing Y. P., Suto Y., 2002, ApJ, 574, 538
Kasun S. F., Evrard A. E., 2005, ApJ, 629, 781
Kelm B., Focardi P., 2004, A&A, 418, 937
Klypin A., Gottlöber S., Kravtsov A. V., Khokhlov A. M., 1999, ApJ, 516, 530
Lee B. C. et al., 2004, AJ, 127, 1811
Lopes P. A. A., de Carvalho R. R., Gal R. R., Djorgovski S. G., Odewahn S. C., Mahabal A. A., Brunner R. J., 2004, AJ, 128, 1017
Macciò A. V., Dutton A. A., van den Bosch F. C., 2008, MNRAS, 391, 1940
Malykh S. A., Orlov V. V., 1986, Astrofizika, 24, 445
Merchán M. E., Zandivarez A., 2002, MNRAS, 335, 216
Merchán M. E., Zandivarez A., 2005, ApJ, 630, 759
Nolthenius R., White S. D. M., 1987, MNRAS, 225, 505
Orlov V. V., Petrova A. V., Tarantaev V. G., 2001, MNRAS, 325, 133
Paz D. J., Lambas D. G., Padilla N., Merchán M., 2006, MNRAS, 366, 1503
Plionis M., Basilakos S., Tovmassian H. M., 2004, MNRAS, 352, 1323
Plionis M., Basilakos S., Ragone-Figueroa C., 2006, ApJ, 650, 770
Ragone-Figueroa C., Plionis M., 2007, MNRAS, 377, 1785
Ramella M., Geller M., Pisani A., da Costa L. N., 2002, AJ, 123, 2976
Robotham A., Phillips S., de Propris R., 2007, ApJ, 672, 834
Sharma S., Johnston K. V., 2009, ApJ, 703, 1061
Springel V., 2005, MNRAS, 364, 1105
Tago E. et al., 2006, Astronomiche Nachrichten, 327, 365
Tago E., Einasto J., Saar E., Tempel E., Einasto M., Vennik J., Muller V., 2008, A&A, 479, 927
Tovmassian H. M., Plionis M., 2009, ApJ, 696, 1441
Tully R. B., 1987, ApJ, 321, 280
van Haarlem M., van de Weygaert R., 1993, ApJ, 418, 544
Wang Y., Yang X., Mo H. J., Li C., van den Bosch F. C., Fan Z., Chen X., 2008, MNRAS, 385, 1511
Wechsler R. H., Bullock J. S., Primack J. R., Kravtsov A. V., Dekel A., 2002, ApJ, 586, 52
Yang X., Mo H. J., van den Bosch F. C., Pasquali A., Li C., Barden M., 2007, ApJ, 671, 153
Yepes G., Sevilla R., Gottlöber S., Silk J., 2007, ApJ, 666, L61

This paper has been typeset from a TEX/LATEX file prepared by the author.